Modeling Atmospheric Refraction Influences by Optical Turbulences Using an Image-Assisted Total Station

Alexander Reiterer

Summary
A large part of geodetic sensor systems use electromagnetic radiation to determine the measurement values (distances, directions, etc.). The geometry of the path of propagation and the velocity of the electromagnetic wave is strongly influenced by the physical state of the atmosphere. As most geodetic measurements are performed in the lower atmosphere, the study of refraction and of corresponding impact constitutes a key research field. In geodesy, the refractive index represents a common way to describe the terrestrial refraction – the literature refers to different methods for determining this value. Our study presents a method for the determination of the influence of refraction on the basis of optical measurements. The mathematical derivation is based on well-known equations – the combination of different approaches leads to a uniform processing sequence which can easily be implemented. We present the theoretical foundations, details about the implementation and some preliminary tests.

Zusammenfassung
Ein großer Teil der geodätischen Messsysteme verwenden elektromagnetische Wellen, um die notwendigen Messwerte (Distanzen, Richtungen etc.) zu bestimmen. Die Geometrie des Ausbreitungsweges und die Geschwindigkeit der elektromagnetischen Welle ist stark vom physischen Zustand der Atmosphäre beeinflusst. Da die meisten geodätischen Messungen in der unteren Atmosphäre durchgeführt werden, stellt das Studium der Refraktion und der entsprechenden Auswirkungen ein zentrales Forschungsfeld dar. In der Geodäsie wird häufig der Brechungsindex verwendet, um die terrestrische Refraktion zu beschreiben – in der Literatur finden sich verschiedene Methoden zur Bestimmung dieses Wertes. Die vorliegende Arbeit basiert auf optischen Messungen zur Bestimmung des Einflusses der Refraktion. Die mathematische Ableitung basiert auf bekannten Gleichungen – die Kombination verschiedener Ansätze führt zu einem einheitlichen Berechnungsalgorithmus. Wir präsentieren die theoretischen Grundlagen, Details über die Implementierung und erste praktische Versuche.

Keywords: Atmospheric Refraction, Optical Turbulence, Image-Assisted Total Station

1 Introduction

The effect of atmospheric refraction presents a fundamental limitation of the accuracy and precision of geodetic measurement methods using electromagnetic radiation. Due to the increasing precision of modern geodetic instruments, considering the influence of refraction is indispensable. In geodesy, the coefficient of refraction k (the ratio of the Earth's radius and the radius of the line of sight) was used in the past to quantify terrestrial refraction. The study of the effect of atmospheric refraction in geodesy is commonly reduced to the determination of the *vertical temperature gradient* $\frac{dT}{dz}$, since k and $\frac{dT}{dz}$ are directly connected.

The vertical temperature gradient, which represents a key descriptive value for the ground-level domain, is influenced by daily variations. As a consequence, the commonly used Gaussian coefficient of refraction of $k = 0.13$ is not representative for the lower atmosphere (surface layer to a height of about 30 m) – from various examinations (Bahnert 1972, Brocks 1939, Eschelbach 2009, Flach 2000, Hirt et al. 2010, Weiss 2002, Wunderlich 1985) typical values between -4 and $+16$ have been investigated.

In geodesy, basing on the ideas of Brunner (1979), several refraction determination methods can be formulated – in the context of refraction-free or refraction-indicated direction measurements, Ingensand (1990) has listed three different approaches: (a) measurement of the dispersion angle, (b) measurement of the temperature gradient, and (c) measurement of turbulence parameters. The **measurement of the dispersion angle** (method a) is a dual-wavelength method, which follows the principle of wavelength-dependent deviation of light (dispersion effect). Emitting and capturing a dual-wavelength laser by a dispersometer makes it possible to calculate the angular difference between the two arriving waves (dispersion angle), which is approximately proportional to the refraction angle. The **acquisition of temperatures or temperature gradients** (method b) can be done directly via suitable sensor systems (e. g. temperature gradient measurement system). The disadvantage of this method is the problem of the representativeness of single temperature (gradient) measurements along the path of light (Hennes et al. 1999, Ingensand 2008). The study at hand is based on the **measurement/derivation of "turbulence parameters"** and the subsequent calculation of the vertical temperature gradient (method c). Several studies have worked out theoretical foundations and implementations of atmospheric turbulence analysis for detecting the influences of refraction, e. g. Brunner (1979), Hennes (1995), Casott (1999), Flach (2000), Eschelbach (2009).

The main goal of the study at hand is to adapt the existing concepts and mathematical derivation. We have formulated an unified process starting with data capturing and ending with the vertical temperature gradient.

Furthermore, the procedure has been validated by practical field experiments (we use a prototype of an image-assisted total station in combination with appropriated image processing techniques).

This paper presents the mathematical foundations (Section 2), describes the measurement system used (Section 3), and presents experimental results and an evaluation of the system and algorithms (Section 4). An outlook (Section 5) concludes the study.

2 Modeling Refraction Influence Using Optical Turbulence

The refractive index n can be described as a random variable affected by the turbulence of the atmosphere (Brunner 1979) and can be divided into a stochastic part and a quasi-static mean part ($n = \bar{n} + n'$) – the same can be applied to the gradient. Using geodetic instrumentation or a scintillometer, the determination of the quasi-static part of the refractive index gradient is possible (Eschelbach 2009).

The *Optical Turbulence Transfer Model* uses two parameters (*turbulence structure parameter* C_n^2 and the *inner scale* l_0) for modeling the energy of turbulence. Based on the fact that an electromagnetic wave is influenced by the turbulence of the atmosphere, these parameters can be determined by the instruments mentioned above. Furthermore, the vertical temperature gradient and subsequently the local coefficient of refraction χ (representing the coefficient of refraction of a particular point) can be calculated by these quantities (*Monin-Obukhov Similarity Theory (MOST)* (Monin & Obukhov 1954)).

The local coefficient of refraction χ is only dependent slightly on air pressure p and air temperature T and can be calculated by (Bahnert 1972)

$$\chi = 503 \frac{p}{T^2} \left(0.0343 + \frac{dT}{dz}\right). \tag{1}$$

The following equations were originally developed by Obukhov (1946), Monin & Obukhov (1954), Brunner (1979), Thiermann (1992), Flach (2000), Eschelbach (2009) – the listing combines these approaches, resulting in a consistent processing sequence. A list of all values including units can be found in Appendix 2.

The calculation starts with the *variance* σ_α^2 of the *angle-of-arrival*, which is given by (Flach 2000)

$$\sigma_\alpha^2 = \frac{\sigma_y^2 \cdot p_x^2}{f^2}, \tag{2}$$

where σ_y^2 is the *variance of the vertical fluctuation of a feature* (measured by image processing methods – see Section 3.2), p_x the *pixel size*, and f the *focal length*. It follows the **turbulence structure parameter** C_n^2 by (Brunner 1979)

$$C_n^2 = \frac{\sigma_\alpha^2 \cdot a^{\frac{1}{3}}}{1.09 \cdot R}, \tag{3}$$

where a is the *aperture of the measurement system* and R the *distance to the object/target* (path length). For the calculation of the **inner scale** l_0 we can use (Flach 2000)

$$l_0 = \frac{\sqrt{\lambda \cdot R}}{y_c}, \tag{4}$$

where λ is the *optical wave length* (e. g. $670 \cdot 10^{-9} m$), and y_c an *auxiliary variable*, which can be derived by (Flach 2000)

$$y_c = -2.692 - 140.5 x_c + 31.86 x_c^{\frac{1}{2}} + 377.8 x_c^{\frac{3}{2}} - 0.317 ln(x_c). \tag{5}$$

The second *auxiliary variable* x_c is given by (Flach 2000)

$$x_c = \frac{\sigma_\chi^2}{C_n^2} \cdot 10^{-12}, \tag{6}$$

where σ_χ^2 is the *logarithmic-amplitude variance*, which can be derived by (Thiermann 1992)

$$\sigma_\chi^2 = \frac{1}{4} \cdot ln\left(\frac{\sigma_I^2}{\langle I \rangle^2} + 1\right). \tag{7}$$

The *auxiliary variables* have been introduced by Flach (2000) reducing the calculation of the relation between the (measured) *logarithmic-amplitude variance* and the *inner scale* to an efficient way. The original equations can be found in Lawrence & Strohbehn (1979).

$\frac{\sigma_I^2}{\langle I \rangle^2}$ represents the *normalised intensity fluctuations* which can be measured by image processing. As mentioned above, p, f and a are parameters given by the sensor used (see Section 3), λ and R depend on the set-up.

On the basis of these formulas we can derive the *vertical temperature gradient*, beginning with the calculation of the *dissipation rate of kinetic energy* ε (Thiermann 1992)

$$\varepsilon = \left(\frac{7.4}{l_0}\right)^4 \cdot v_{kin}^3, \tag{8}$$

where v_{kin} is the *kinematic viscosity of air* ($15.6 \cdot 10^{-6} \frac{m^2}{s}$ for a temperature of 293.15 K and an air pressure of 1000 hPa). Subsequently, the *structural parameter of temperature* C_T^2 can be calculated by (Thiermann 1992)

$$C_T^2 = \left(\frac{\overline{T}^2}{A_\lambda \cdot \overline{p}}\right)^2 \cdot C_n^2, \tag{9}$$

where A_λ is a parameter which has to be chosen depending on the optical wave length λ (e. g. $A_\lambda = 7.8 \cdot 10^{-5} \frac{K}{hPa}$

for $\lambda = 670 \cdot 10^{-9} m$ to $940 \cdot 10^{-9} m$), $\overline{T}$ the *mean air temperature*, and $\overline{p}$ the *mean air pressure*.

For the following calculation we assume that the *dynamic atmospheric stratification* is unstable. The *friction velocity* u_* can be derived by (Monin & Obukhov 1954, Eschelbach 2009)

$$u_* = \left(\frac{\varepsilon k z}{(1-3\zeta)^{-1} - \zeta} \right)^{\frac{1}{3}} , \tag{10}$$

where k is the dimensionless *von Kármán constant*, describing the logarithmic velocity profile of the turbulent flow (typically the value 0.41 is used), z the *height of the optical propagation path*, and ζ a dimensionless *stability parameter*, which itself can be calculated by (Monin & Obukhov 1954)

$$\zeta = \frac{z}{L} . \tag{11}$$

ζ can be used for the classification of the dynamic atmospheric stratification (e. g. $\zeta < 0$ means that the dynamic atmospheric stratification is unstable).

The stability of the surface layer can be described by the *Obukhov length* L (Obukhov 1946)

$$L = \frac{\overline{\theta} u_*^2}{k g T_*} , \tag{12}$$

where the *temperature scale factor* T_* is defined by (Monin & Obukhov 1954, Eschelbach 2009)

$$T_* = \left(\frac{C_T^2 (kz)^{\frac{2}{3}}}{\phi_{C_T}} \right)^{\frac{1}{2}} , \tag{13}$$

with the *universal function of the structural parameter of temperature* ϕ_{C_T} defined by (Thiermann 1992)

$$\phi_{C_T} = 4\beta_1 (1 - 7\zeta + 75\zeta^2)^{-\frac{1}{3}} . \tag{14}$$

β_1 is the *Obukhov-Corrsin constant* (= 0.86). In Eq. 12, $\overline{\theta}$ represents the *mean potential temperature*, which can be calculated by (Stull 1988)

$$\overline{\theta} = \overline{T} \left(\frac{1000}{\overline{p}} \right)^{0.286} . \tag{15}$$

The calculation of Eq. 10, 11, 12, 13 has to be done iteratively, starting with $\zeta = 0$. Subsequently, the *vertical temperature gradient* $\frac{dT}{dz}$ can be derived by (Webb 1984)

$$\frac{dT}{dz} = -\frac{T_* \phi_T}{kz} , \tag{16}$$

where

$$\phi_T = 0.74 \, (1 - 9\zeta)^{-\frac{1}{2}} . \tag{17}$$

Deussen (2000) has shown that the *vertical temperature gradient* mainly depends on the *turbulence structure parameter* C_n^2. Periods with low turbulence (C_n^2 between 10^{-16} and $10^{-14} m^{-\frac{2}{3}}$) result in a vertical temperature gradient lower than $0.1 \frac{K}{m}$, periods with medium turbulence (C_n^2 between 10^{-14} and $10^{-13} m^{-\frac{2}{3}}$) yield a gradient of $0.2 \frac{K}{m}$, and for periods with strong turbulence ($C_n^2 > 10^{-13}$) values up to $0.5 \frac{K}{m}$ are possible. During strong turbulence a halving of l_0 from 6 *mm* to 3 *mm* leads to an increase of the *vertical temperature gradient* of $0.11 \frac{K}{m}$.

One of the main problems calculating the vertical temperature gradient by using the *Monin-Obukhov Similarity Theory* is that the derivation shown above is valid only in the homogeneous surface layer. They assume that the flow is steady-state, horizontal and homogeneous, and in equilibrium with the underlying surface.

Eschelbach (2009) has formulated an alternative approach, taking into account that geodetic measurements are almost always carried out on non-homogeneous terrain. ϕ_{C_T} (given in Eq. 14) can be replaced by

$$\phi_{C_T} = 4\beta_1 \phi_H (\phi_M - \zeta)^{-\frac{1}{3}} , \tag{18}$$

where the *universal functions* ϕ_M and ϕ_H are given by (Eschelbach 2009)

$$\phi_M = (1 - 3\zeta)^{-1} \quad \textit{and} \quad \phi_H = 0.95 (1 - 11.6\zeta)^{-\frac{1}{2}} . \tag{19}$$

The literature (Businger et al. 1971, Thiermann 1992, Weiss 2002, Eschelbach 2009) refers to different equations for calculating ϕ_M and ϕ_H. The selection can be made on the basis of the type of stability parameters of stratification (analysing the value of ζ). Eq. 19 was originally formulated by Businger et al. (1971) and is valid for $\zeta < 0$.

On the basis of ϕ_{C_T} from Eq. 18 new values for u_*, ζ, T_*, L, and subsequently a vertical temperature gradient can be calculated, which applies to non-homogeneous terrain with low wind speed.

3 Measurement and Analysis System

The study at hand uses an image-based measurement system combined with appropriate processing algorithms to derive the *turbulence structure parameters*, the *inner scale*, and subsequently the *vertical temperature gradient*. To evaluate the derived results we used a displaced-beam scintillometer as a reference system. In the following section we will provide some basic information about sensor systems and processing algorithms.

3.1 Sensor Systems

Displaced-Beam Scintillometer

Displaced-beam scintillometers determine the structural parameter of optical turbulence using a laser beam. The

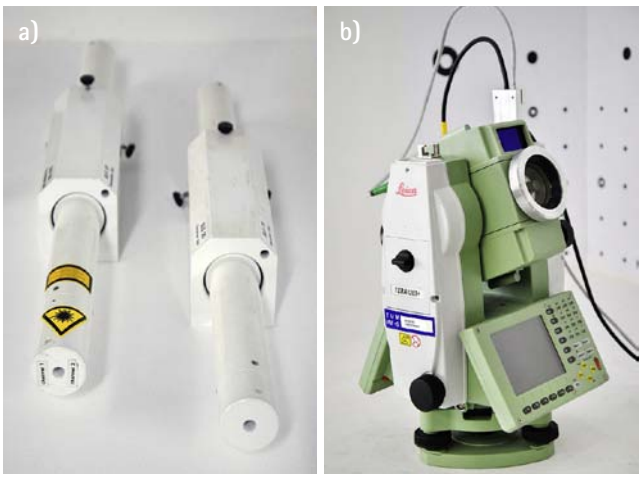

Fig. 1: Used measurement systems: a) displaced-beam scintillometer (transmitter and receiver), b) image-assisted total station

work at hand is based on the Scintec SLS20 scintillometer (Fig. 1a), which is able to derive both *turbulence structure parameter* C_n^2 and *inner scale* l_0 (Thiermann 1992). Furthermore, the system is able to derive the *sensible heat flux*, the *momentum flux*, and the *Obukhov length (L)*. The SLS20 emits two laser beams (parallel, differently polarised) with a known separation (d). After having penetrated the atmosphere (over a path of 50 to 250 m) the two laser beams are identified by their polarisation in the receiver. The emitted beams are influenced by the random fluctuation of refractivity in the atmosphere, resulting in fluctuation of the intensity of the received signal. The variance and covariance of these intensity values are used to derive C_n^2 and l_0.

The SLS20 works with an optical wavelength of 670 nm, and a beam divergence of 3×8 mrad. To capture data sets, the length of the main data period (MDP) and the length of the diagnosis data period (DDP) have to be specified. It is important to know that MDP must be long enough to achieve a statistically significant sample. However, an excessively long period leads to data loss in the case of an error – a typical value is 6 seconds. MDP is the averaging time for taking data and should ideally be a multiple of DDP (a commonly used value is 60 seconds). A detailed description of the SLS20 can be found in Thiermann (1992) and Flach (2000).

Image-Assisted Total Station (IATS)

Image-assisted total stations offer the user an image capturing system (CCD/CMOS camera) in addition to 3D point measurements. Several developments and applications of IATS have been published, e. g. Reiterer (2004), Walser (2004), Vicovac (2008), Wasmeier (2009).

The study at hand uses an IATS (Fig. 1b), which is based on a Leica Geosystem 1200 total station with a colour CMOS camera ($\frac{1}{2}$ inch, 2560×1920 pixel, with a pixel size (p_x) of 2.2×2.2 μm) in the optical path. The focal length (f) is 228.5 mm, resulting in a field-of-view of 1.56×1.17 gon. One pixel on the image sensor corresponds to an angular value of 0.61 mgon. The objective lens aperture (a) is 40 mm. A detailed description of the IATS used can be found in Wasmeier (2009) and Reiterer & Wagner (2012).

General information about the necessary precision of *vertical fluctuation of a feature* and the *intensity fluctuation* to obtain the *vertical temperature gradient* and the *local coefficient of refraction* with a certain uncertainty can hardly be achieved. Flach (2000) has estimated the preconditions to measure the refraction influences by optical turbulence by

$$\sigma_{C_n^2} = \frac{a^{\frac{1}{3}}}{1.09R}\sigma_{\sigma_\alpha^2}. \tag{20}$$

Adapting this estimation for our measurement system leads to a standard deviation for the angle-of-arrival $\sigma_{\sigma_\alpha^2}$ of $7.7 \cdot 10^{-12}$ rad^2.

A second important criterion for the calculation of the *turbulence structure parameter* and the *inner scale* is the frame rate of the image capturing process. Casott (1999) has formulated a minimal capturing frequency of 150 Hz – lower frequencies result in an insufficient capturing of the (vertical and intensity) fluctuations and therefore in an imprecise determination of the vertical temperature gradient.

The maximum frame rate (MFR) in our system depends on the selected resolution of the image. By adapting the image size, MFR can be increased, e. g. capturing full-frame images results in an MFR of 5 Hz, whereas an image size of 144×144 pixel leads to an MFR of 200 Hz.

3.2 Analysis System

Scintillation-Based Measurement Method

For analysing measurements from displaced-beam scintillometers the same principles as described in Section 2 can be applied. The scintillation-based measurement method is based on the comparison of the scintillation of two laser beams measured over two close, parallel propagation paths. The fluctuation of the intensity of the beams is measured at the receiver. The correlation of the logarithmic-amplitude r_χ can be derived by (Thiermann 1992)

$$r_\chi = \frac{B_{1,2}}{\sigma_\chi^2} = f(l_0, a, d, R)\ , \tag{21}$$

where a is the *aperture of the scintillometer* (receiver), d the *beam separation*, and R the *length of the path*. The *covariance of logarithmic-amplitude* of the two laser beams $B_{1,2}$ is given by

$$B_{1,2} = 4\pi^2 K^2 \int_0^R \int_0^\infty k\Phi_n(k, l_0, C_n^2) J_0(kd) \\ sin^2\left[\frac{k^2 x(R-r)}{2kR}\right]\left[\frac{(4J_1^2)\frac{kar}{2R}}{(\frac{kar}{2R})^2}\right] dkdr. \tag{22}$$

k is the *wave number of radiation*, K the *wave number of the scintillometer* ($K = \frac{2\pi}{\lambda}$) ,Φ_n the *decay of refractive index fluctuation in dissipation sub-range*, r a *coordinate along the propagation path*, and J_0 and J_1 *Bessel functions*. Eq. 21 is a function of C_n^2, the l_0 and the known instrument values; a resolution for C_n^2 is easily possible using the intensity variance of only one simple path. A detailed description of the mathematical derivation can be found in Thiermann (1992) and Weiss (2002).

Image-Based Measurement Method

Traditional total stations are based on point-oriented measurement techniques: signalized or natural targets are measured to reconstruct, monitor or track an object. Using an IATS the procedure of measurement can be extended by automated methods for recognizing features on objects. Reiterer & Wagner (2012) have implemented and evaluated three different approaches for capturing objects: an edge-based, template-based, and point-based method. The study has shown that the edge-based method is the most precise – the combination of IATS and edge detection is able to measure objects with a standard deviation of 0.04 pixel, which corresponds to 0.024 mgon (with an uncertainty of $\pm 0.04 \cdot \sigma$).

The work at hand uses the edge detection algorithm as described by Reiterer & Wagner (2012). Edge extraction is performed to a region-of-interest (ROI) which contains the horizontal structure of the target. This pre-selection has the main advantage that the relevant edges can be easily selected, and that a reduced domain is an efficient way to speed up the process. As result we get the vertical sub-pixel coordinates of the extracted edge. Capturing more than one image enables us to calculate the variance of the vertical fluctuation of an edge (feature) over time.

In addition to the vertical variation of a feature, the fluctuation of the intensity of the signal also has to be measured. Deussen (2000) and Flach (2000) have used a *Wiener Filter* (normally used for noise filtering and deblurring) to derive $\frac{\sigma_I^2}{\langle I \rangle^2}$. A disadvantage of this approach is the huge number of calculations necessary – given that we have about 9.000 images per analysis period and assuming that this procedure has to be real-time capable, the *Wiener Filter* is not a suitable algorithm (on up-to-date hardware the processing of one data period requires about 80 seconds). Therefore, the study at hand uses the estimation of the spectrum of noise to determine the intensity fluctuations (Buckley 1994). In a first step, the signal is processed by a thin-plate smoothing spline

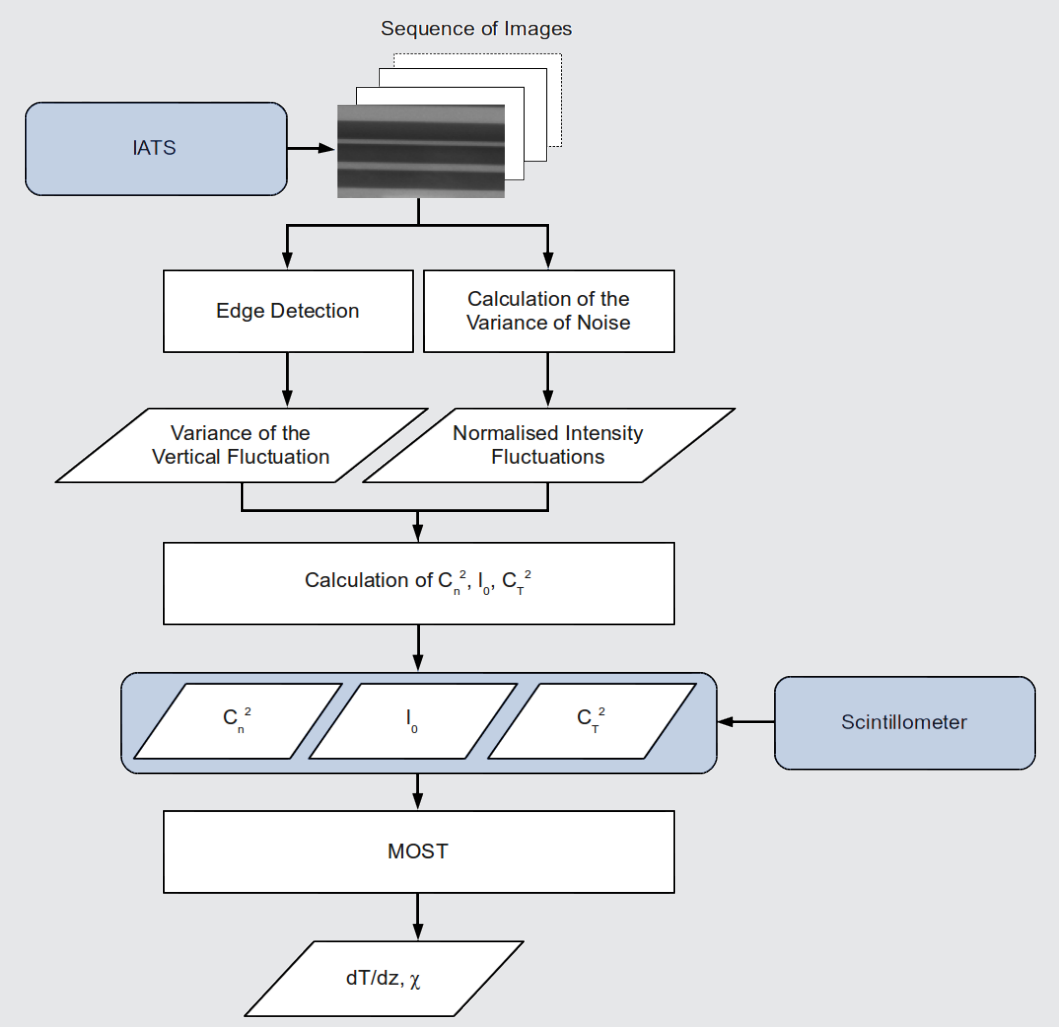

Fig. 2: Overview of the processing sequence for determining the vertical temperature gradient $\frac{dT}{dz}$ and the local coecient of refraction χ.

model. In a second step the model, whose generalized cross-validation score is minimum, is assumed to be able to provide the variance of the additive noise, which can be used as a measure for the intensity fluctuation. A comparison between the *Wiener Filter* and the used *estimation of the spectrum of noise* shows maximal differences of $6 \cdot 10^{-4}$ for the intensity fluctuation. Therefore, for the used test data the two approaches can be described as equivalent. Future tests have to demonstrate the applicability of the presented procedure.

The measured vertical edge fluctuations and the intensity fluctuations can be used directly for Eq. 2 and Eq. 7. Subsequently, the vertical temperature gradient $\frac{dT}{dz}$ and the local coefficient of refraction χ can be derived as described in Section 2. An overview of the processing sequence is shown in Fig. 2.

4 Experiments: Measurements and Results

In order to validate the measurement and processing sequence, several field tests have been carried out. The experiments were realized in October 2011 on a grassy field at the Max-Kneissl-Institute (Chair of Geodesy, Technische Universität München) near Munich. The measurement area is approximately flat and enclosed by trees (see Fig. 3). The measurement set-up consists of an IATS, a scintillometer, and a temperature sensor (PT 100). The line of sight of both instruments runs horizontally over a distance of 75 m (*path length, R*). The temperature sensor was placed in the middle of the path at a height of 1.1 m (*height of the line of sight, z*). As target a sheet consisting of horizontal bars was used – one of these bars served for edge detection.

During the first day of measurement (which is shown in the following) the weather was sunny (clear) with temperature values between 16°C and 21°C and a mean air pressure of 955 hPa. The total measurement period lasted 8 hours. Images were captured with 150 Hz, which results

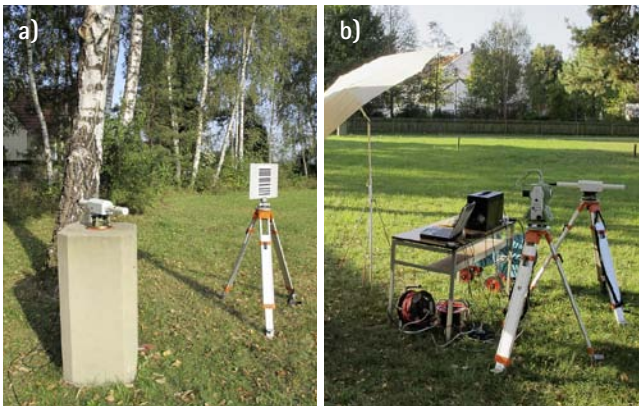

Fig. 3: Measurement set-up with IATS and scintillometer working in parallel: a) transmitter and target, b) receiver and IATS

in 9.000 images for a data period of 1 minute. The measurements were repeated every 10 minutes, which yielded 43 measurement periods. The value for the main data period of the scintillometer was set to 1 minute to have comparable results.

The captured images have been used for edge detection and subsequent calculation of the *variance of the vertical fluctuation* (σ_y^2) – the first image (one horizontal bar) of each series has been defined as a reference. Additionally, the *normalised intensity fluctuations* ($\frac{\sigma_I^2}{\langle I \rangle^2}$) were derived as described above. During image capturing, problems arose due to animals (flies, gnats, etc.) crossing the line of sight. These 'disturbing objects' led to a failure of edge detection – corresponding images were therefore excluded from processing by manual selection.

Fig. 4a and 5a show C_n^2 and l_0 calculated from IATS measurements and measured by the scintillometer. To have a benchmark for the similarity of the reference and the derived values the corresponding correlations are shown in Fig. 4b and 5b.

The *turbulence structure parameter* C_n^2 increases during the first hours of the measurement, peaking a maximum at 11:20. The correlation between scintillometer measurements and derived values from IATS is 0.95 – this result is comparable to the study of Flach (2000). The correlation in the first three hours can be described as excellent. Between 12:30 and 14:00 there were slightly higher deviations, which can be explained by the different positions of the two systems and the varying cast shadow coming from trees. From 14:00 onwards the two curves drift further apart – the value which was derived by IATS measurements exhibits considerably higher peaks than the scintillometer measurements. The deviations do not exceed a maximum of $0.27 \cdot 10^{-13} m^{-\frac{2}{3}}$.

Analysing the inner scale l_0 (Fig. 5a) shows that the highest values were reached in the morning (at 8:30 a value of 7.9 mm), decreasing down to 4.5 mm in the afternoon. It is also clearly visible, that the correlation between scintillometer measurements and derived values from IATS is lower than for C_n^2 ($r_{corr} = 0.72$). Note at 10:30 the sudden fall of l_0 by 2 mm. This can be explained by the change of the wind characteristics – in our case by an increase of wind speed. From 10:30 to 14.00 there is a strong correlation between the two measurement series, while from 14:00 there is a stronger divergence (the scintillometer gives values which are up to 1 mm higher for l_0) – explainable by varying cast shadows (see above).

Due to the fact that our study does not use any information or measurement concerning wind speed, the influence factors were not considered. Typically, high values for l_0 can be found in time periods where the wind speed is low which we expect.

The vertical temperature gradient show that (for our measurement data) the differences between the values derived by the MOST and the extended MOST (Eq. 18 and 19) are negligible ($\Delta_{max} = 0.008 \frac{K}{m}$). Therefore, we will discuss the result of the traditional MOST only.

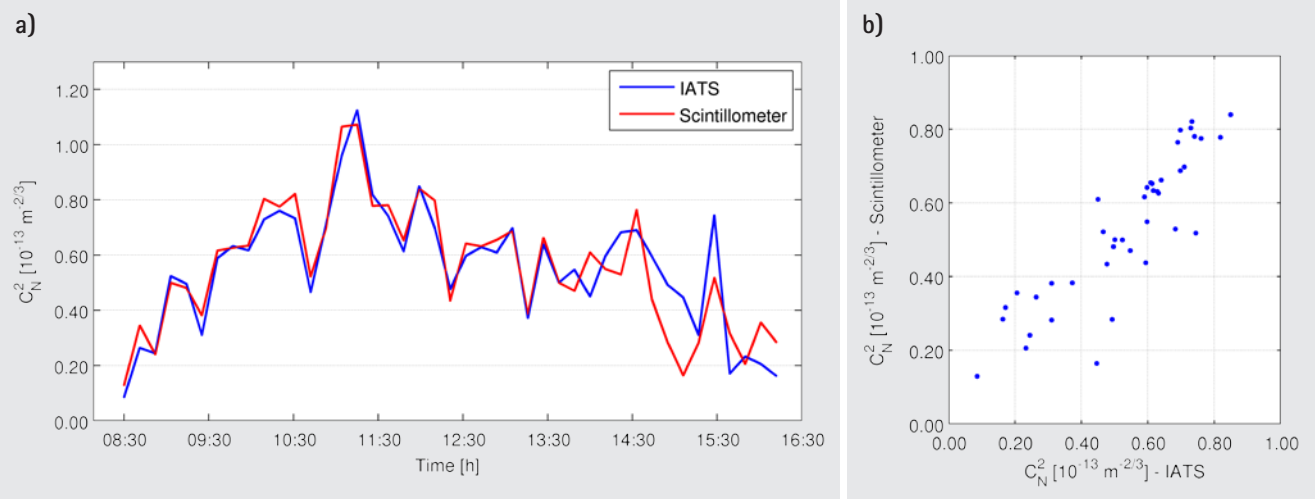

Fig. 4: a) Time series of the turbulence structure parameter C_n^2 , and b) corresponding correlations (6.10.2011)

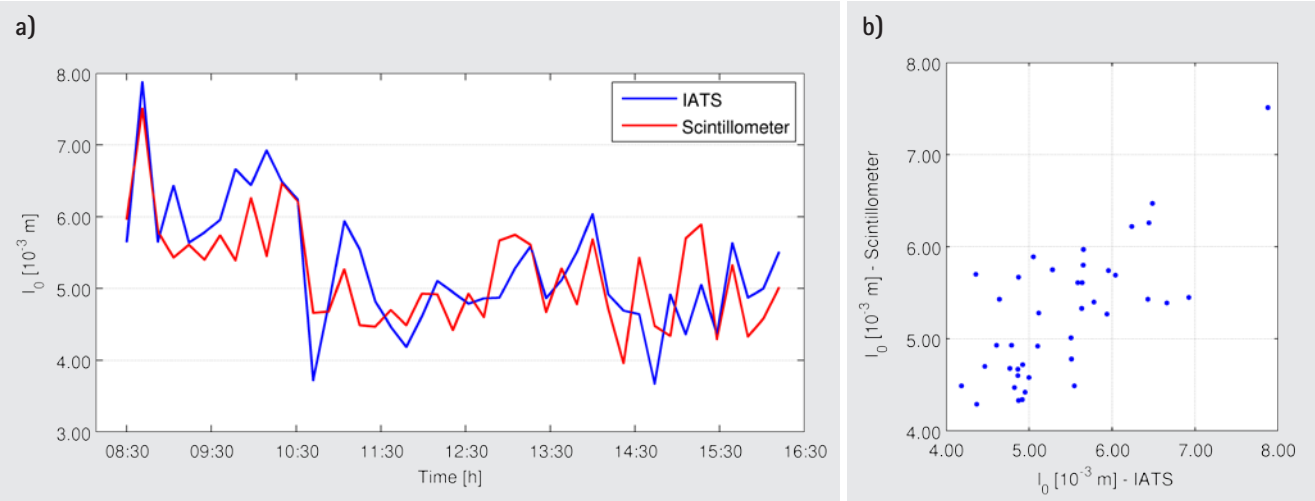

Fig. 5: a) Time series of the inner scale l_0, and b) corresponding correlations (6.10.2011)

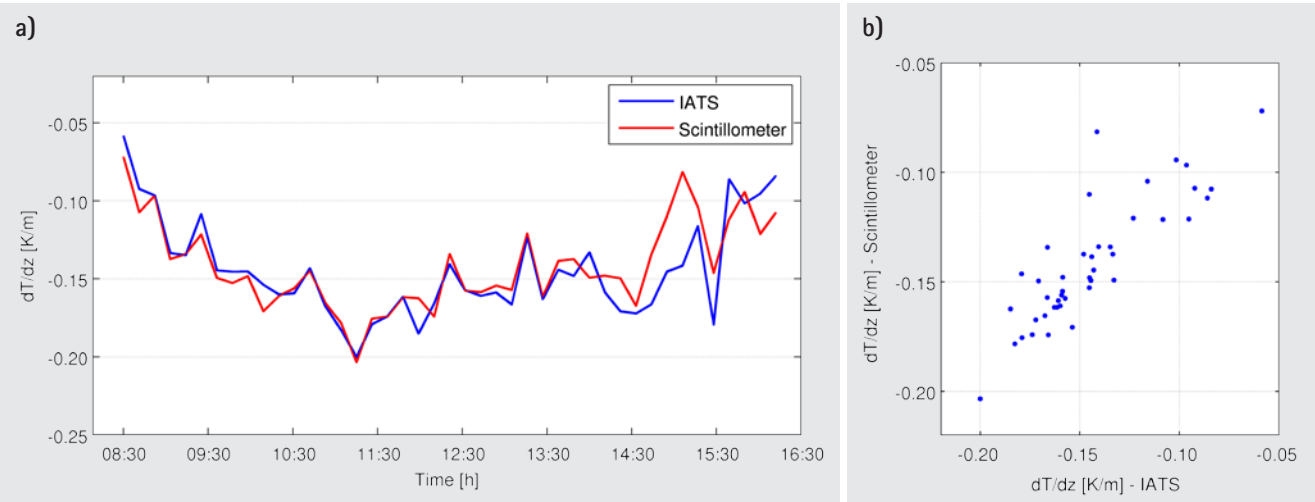

Fig. 6: a) Temperature gradient derived from IATS and scintillometer measurements, and b) corresponding correlations (6.10.2011)

The vertical temperature gradient derived from measurements of IATS and scintillometer amounts to a correlation r_{corr} of 0.85 – the result is shown in Fig. 6. Between 8:30 and 14:00 the two gradients fit very well ($r_{corr} = 0.93$), followed by a period with differences up to 0.06 $\frac{K}{m}$. Note that $\frac{dT}{dz}$ is derived on the basis of C_n^2 and l_0, and both values differ considerably from the reference after 14:00 (cp. Fig. 4 and 5).

It is clearly visible that the influence of l_0 is considerable smaller than that of C_n^2. Periods, in which the C_n^2 derived from IATS measurements clearly differs from the scintillometer measurements, lead directly to larger deviations of the two measurement series (cp. data set at 15:00), whereas a large difference of the two derived l_0-values has only a minor influence on the vertical temperature gradient (cp. data set at 10:00). Deussen (2000) has shown that for $\frac{dT}{dz}$ between -0.02 $\frac{K}{m}$ and -0.50 $\frac{K}{m}$ the influence of l_0 on the vertical temperature gradient reaches a maximum of 20%.

Note that a second data set (temperature values between 1°C and 13°C and a mean air pressure of 952 hPa) including the derived vertical temperature gradient is shown in Appendix 1. The data show the same characteristics as the example above – C_n^2 can be modeled relatively well ($r_{corr} = 0.91$), whereas l_0 can be reproduced with a decreased correlation ($r_{corr} = 0.65$).

It can be summarized that IATS measurements and the presented procedure can be used to model the turbulence structure parameter C_n^2 with a very high level of precision (in relation to a reference determined by a scintillometer) ($r_{corr} > 0.90$). The inner scale l_0, which is particularly influenced by the wind-speed and the wind-direction, can be modeled with a correlation of around 0.70. Recording wind characteristics (as proposed by e. g. Eschelbach 2009) appears to be indispensable for reliable modelling of l_0 and thus for a reliable derivation of $\frac{dT}{dz}$ from optical turbulences. Measuring the wind characteristics becomes particularly important for periods with low wind speed ($< 0.3\ m/s$ – see Deussen 2000). Special attention performing practical test with both IATS and scintillometer should be be given on identical/comparable environment characteristics (line of sight, cast shadows, wind characteristics, etc.).

5 Conclusions and Outlook

This paper proves that the determination of the influence of the refraction on the basis of IATS measurements is possible. Experiments confirm the approach developed by Brunner (1979), Flach (2000), Eschelbach (2009). The presented modeling is restricted to horizontal and homogeneous surfaces – future research work will focus on the development of new methods which permit the extension of the practical case (e. g. longer path length, inclined terrain situations) – an adaptation of the profile functions used will be necessary (Eq. 14, 18, 19). Furthermore, equipment has to be extended by a vertical temperature gradient measurement system and an anemometer (for measuring wind speed and direction). Nevertheless, the algorithms and methods presented here will be evaluated based on a large number of experiments, and under various conditions.

However, geodetic applications like object monitoring are mostly based on the measurement of points. Reiterer & Wagner (2012) have introduced and evaluated a point-based measurement method which could be used for detecting the variance of the vertical fluctuation (e. g. for predefined structures or features). Theoretically, the precision of the detection methods should be adequate for deriving the necessary parameter – further tests will reveal the practicability and feasibility of this approach. The advantage would be that the calculation of the variance of the vertical fluctuation should be possible on the basis of natural structures without using an artificial target.

Acknowledgement

The research presented in this paper has been supported by the *Alexander von Humboldt Foundation*. Furthermore, we would like to thank the *Institute of Geodesy and Photogrammetry* of *ETH-Zurich* for providing a displaced-beam scintillometer.

References

Bahnert, G.: Bestimmung und Verwendung vertikaler Temperaturgradienten. In: Vermessungstechnik, Vol. 5, 1972.

Brocks, K.: Vertikaler Temperaturgradient und terrestrische Refraktion insbesondere im Hochgebirge. Veröffentlichung des Institutes für Meteorologie der Universität Berlin, 1939.

Brunner, F. K.:Vertical Refraction Angle Derived from the Variance of the Angle-Of-Arrival Fluctuations. In: Refractional Influences in Astronomy and Geodesy, Tengström, E., Teleki, G. (Eds.), pp. 227–238, 1979.

Buckley, M. J.: Fast Computation of a Discretized Thin-Plate Smoothing Spline for ImageDdata. Biometrika, Vol. 81/2, pp. 247–258, 1994.

Businger, J. A., Wyngaard, J. C., Izumi, Y., Bradley, E. F.: Flux-Prole Relationships in the Atmospheric Surface Layer. Journal of the Atmospheric Sciences, Vol. 28, pp. 181–189, 1971.

Casott, N.: Erfassung des Einflusses der ›turbulenten Refraktion‹ auf optische Richtungsmessungen mit CCD-Sensoren. PhD Thesis, Friedrich-Wilhelms-Universität Bonn, 1999.

Deussen, D.: Messverfahren zur Erfassung der Vertikalrefraktion unter Nutzung der atmosphrischen Turbulenzen. Shaker Verlag, Aachen, 2000.

Eschelbach, C.: Refraktionskorrekturbestimmung durch Modellierung des Impuls- und Wärmeflusses in der Rauhigkeitsschicht. KIT Scientic Publishing, 2009.

Flach, P.: Analysis of Refraction Influences in Geodesy Using Image Processing and Turbulence Models. PhD Thesis, ETH-Zurich, 2000.

Hennes, M.: Entwicklung eines Messsystems zur Ermittlung von Turbulenzparametern der Atmosphäre für Anwendungen in der Geodäsie. PhD Thesis, University of Bonn, 1995.

Hennes, M., Dnicke, R., Christ, H.: Zur Bestimmung der temperaturgradienteninduzierten Richtungsverschwenkung beim Tunnelvortrieb. Vermessung, Photogrammetrie, Kulturtechnik (VPK), Vol. 8, pp. 418–426, 1999.

► To be continued on page 165.

Appendix 1

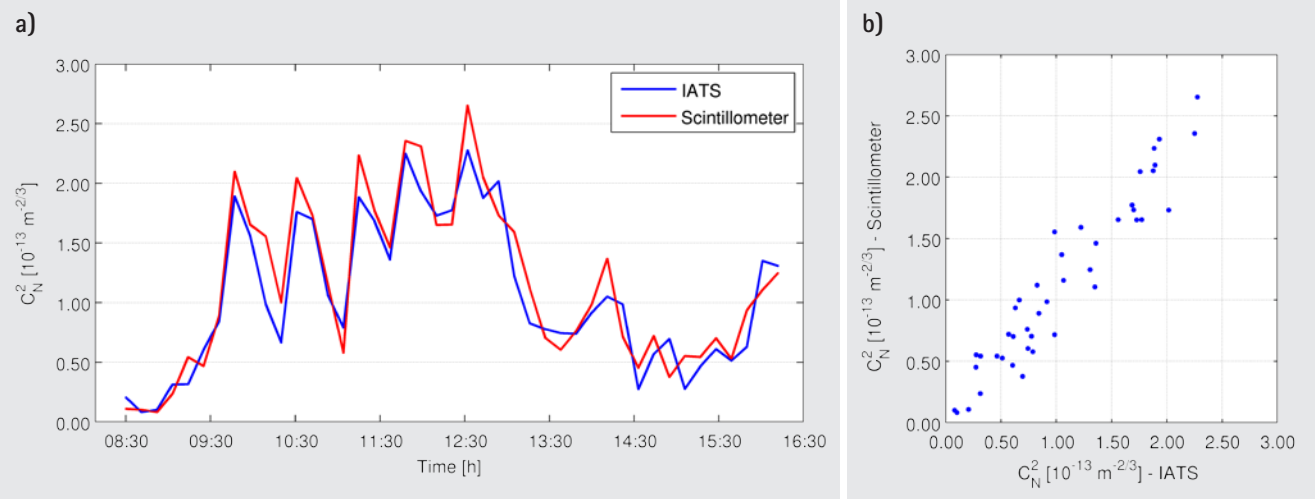

Fig. 7: a) Time series of the turbulence structure parameter C_n^2 , and b) corresponding correlations (24.10.2011)

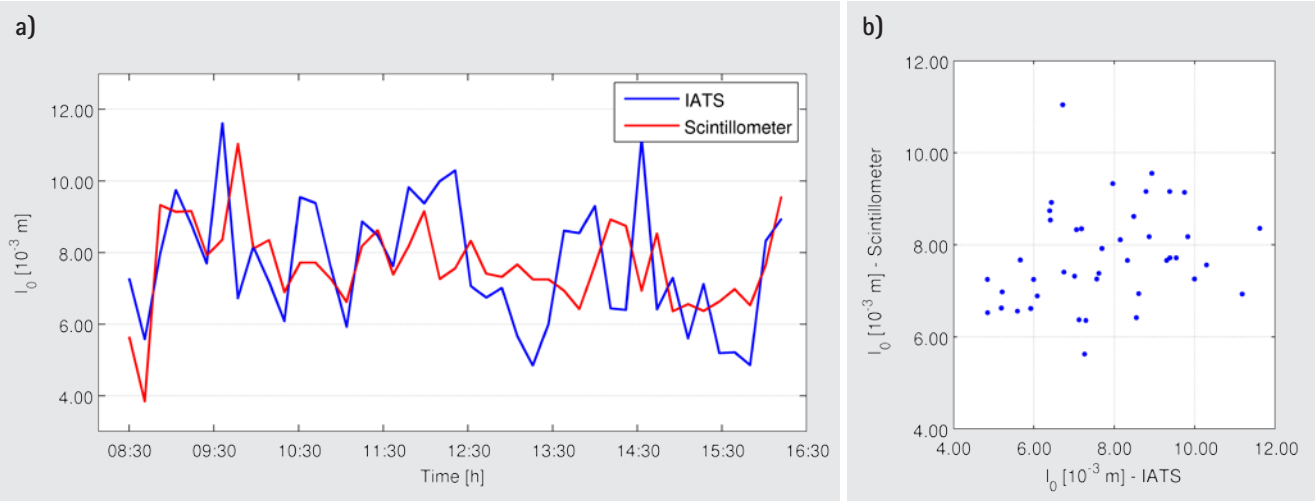

Fig. 8: a) Time series of the inner scale l_0, and b) corresponding correlations (24.10.2011)

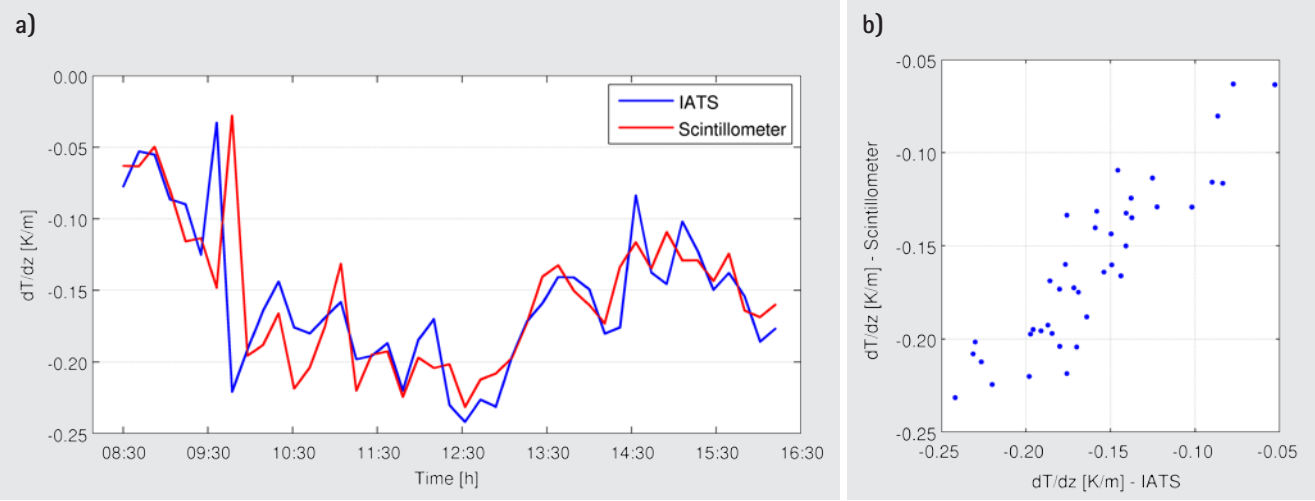

Fig. 9: a) Temperature gradient derived from IATS and scintillometer measurements, and b) corresponding correlations (24.10.2011)

Appendix 2

σ_α^2	variance of the angle-of-arrival	$[rad]$
σ_y^2	variance of the vertical fluctuation	$[pixel^2]$
p_x	pixel size	$[m]$
f	focal length	$[m]$
C_n^2	turbulence structure parameter	$[m^{-\frac{2}{3}}]$
a	aperture	$[m]$
R	distance to the object/target (length of path)	$[m]$
l_0	inner scale	$[m]$
λ	optical wave length	$[m]$
x_c, y_c	auxiliary variables	[ ]
σ_χ^2	logarithmic-amplitude variance	[ ]
$\frac{\sigma_I^2}{\langle I \rangle^2}$	normalized intensity fluctuation	[ ]
ε	dissipation rate of kinetic energy	$[\frac{m^2}{s^3}]$
v_{kin}	viscosity of air	$[\frac{m^2}{s}]$
C_T^2	structure parameter of temperature	$[K^2 m^{-\frac{2}{3}}]$
T, $\overline{T}$	(mean) air temperature	$[K]$
A_λ	parameter depending on the optical wave length	$[\frac{K}{hPa}]$
p, $\overline{p}$	(mean) air pressure	$[hPa]$
u_*	friction velocity	[ ]
k	von Kármán constant	[ ]
z	high of the optical propagation path	$[m]$
ζ	stability parameter	[ ]
L	Obukhov length	$[m]$
θ, $\overline{\theta}$	(mean) potential temperature	$[K]$
g	gravitation constant	$[\frac{m}{s^2}]$
T_*	temperature scale factor	[ ]
ϕ_{C_T}	structural parameter of temperature	[ ]
β_1	Obukhov-Corrsin constant	[ ]
$\frac{dT}{dz}$	vertical temperature gradient	$[\frac{K}{m}]$
ϕ_T	profile function	[ ]
ϕ_H, ϕ_M	universal functions	[ ]
χ	coefficient of refraction of a specific point	[ ]
r_χ	correlation of the logarithmic-amplitude	[ ]
$B_{1,2}$	covariance of the logarithmic-amplitude	[ ]
d	beam separation	$[m]$
k	wave number of radiation	[ ]
K	wave number of the scintillometer	[ ]
Φ_n	decay of refractive index fluctuation in dissipation sub-range	[ ]
r	coordinate along the propagation path	$[m]$
J_0, J_1	Bessel functions	[ ]

▸ Continued from page 163.

Hirt, C., Guillaume, S., Wisbar, A., Brki, B., Sternberg, H.: Monitoring of the Refraction Coefficient in the Lower Atmosphere Using a Controlled Setup of Simultaneous Reciprocal Vertical Angle Measurements. In: Journal of Geophysical Research, Vol. 115, 2010.

Ingensand, H.: Das Rapid Precision Levelling Projekt – Die Entwicklung eines automatisierten trigonometrischen Nivellementsystems mit integriertem Dispersometer. Vermessungswesen und Raumordnung, Vol. 52(2+3), pp. 105–114, 1990.

Ingensand, H.: Concept and Solutions to Overcome the Refraction Problem in Terrestrial Precision Measurement. In: Geodesy and Cartography, Vol. 34(2), pp. 61–65, 2008.

Lawrence, R. S., Strohbehn, J. W.: A Survey of Clear-Air Propagation Effects Relevant to Optical Communications. In: Proceedings of the IEEE, Vol. 58(10), pp. 1523–1545, 1970.

Monin A. S., Obukhov A. M.: Basic Laws of Turbulent Mixing in the Atmosphere Near the Ground. In: Academiia Nauk, SSSR, Geozicheskogo Instituta, Vol. 24, No. 151, 1954.

Obukhov, A. M.: Turbulence in an Atmosphere with a Non-Uniform Temperature. Translation in Boundary Layer Meteorology, 1946.

Reiterer, A.: A Knowledge-Based Decision System for an On-Line Videotheodolite-Based Multisensor System. PhD Thesis, Vienna University of Technology, 2004.

Reiterer A., Wagner, A.: System Considerations of an Image-Assisted Total Station – Evaluation and Assessment. In: Allgemeine Vermessungsnachrichten (AVN), Vol. 3, pp. 83–94, 2012.

Thiermann, V.: A Displaced-Beam Scintillometer for Line-Averaged Measurements of Surface Layer Turbulence. In: Proceedings of the 10th Symposium on Turbulence and Diffusion, 1992.

Stull, R. B.: An Introduction to Boundary Layer Meteorology. Springer, 1988.

Vicovac, T.: Evaluierung der Leica IATS für die konkrete Aufgabenstellung der on-line Objektrekonstruktion. Diploma Thesis, Vienna University of Technology, 2008.

Walser, B.: Development and Calibration of an Image Assisted Total Station. PhD Thesis, ETH-Zurich, 2004.

Wasmeier, P.: Grundlagen der Deformationsbestimmung mit Messdaten bildgebender Tachymeter. PhD Thesis, Technische Universität München, 2009.

Webb, E. K.: Temperature and Humidity Structure in the Lower Atmosphere. In: Geodetic Refraction, Brunner, F. K. (Ed.), pp. 85–141, 1984.

Weiss, A.: Determination of Thermal Stratication and Turbulence of the Atmospheric Surface Layer Over Various Types of Terrain by Optical Scientillometry. PhD Thesis, ETH-Zurich, 2002.

Wunderlich, T.: Die voraussetzungsfreie Bestimmung von Refraktionswinkeln. In: Geowissenschaftliche Mitteilungen, Vol. 26, Vienna University of Technology, 1985.

Author's address
Dipl.-Ing. Dr. techn. Alexander Reiterer
Lehrstuhl für Geodäsie
Technische Universität München
Arcisstraße 21, 80333 München